Stapp Car Crash Journal, Vol. 55 (November 2011), pp. 479-490

2011-18

Patterns of Acetabular Femoral Head Coverage

Sven Holcombe, Carla Kohoyda-Inglis, Lu Wang, James A. Goulet, Stewart C. Wang
University of Michigan

Richard W. Kent
University of Virginia

ABSTRACT – The size and shape of the acetabulum and of the femoral head influence the injury tolerance of the hip joint. The aim of this study is to quantify changes in acetabular cup geometry that occur with age, gender, height, and weight. Anonymized computed tomography (CT) scans of 1,150 individuals 16+ years of age, both with and without hip trauma, were used to describe the acetabular rim with 100 equally spaced points. Bilateral measurements were taken on uninjured patients, while only the uninjured side was valuated in those with hip trauma. Multinomial logistic regression found that after controlling for age, height, weight, and gender, each 1 degree decrease in acetabular anteversion angle (AAA) corresponded to an 8 percent increase in fracture likelihood (p<0.001). Age, weight, and gender were found to influence anteversion angle significantly, with each 10 years in age increasing AAA by 1.07 degrees, each 10kg of weight decreasing AAA by 0.45 degrees, and being female resulting in 1.42 degrees greater AAA than males. Height was not found to relate significantly to AAA after other anthropometric factors were controlled for. Height, age, and weight, however, correlated with femoral head radius, thus establishing a relationship with acetabular rim size independent of rim shape. A parametric model of the 3D acetabular rim landmark points is reported, allowing for the creation of individualized acetabular geometry for any given age, gender, height, and weight. A custom-built tool to produce such geometry programmatically is also provided.

KEYWORDS – (Pelvis, Acetabulum, Acetabular geometry, Acetabular fracture, CT, Anteversion)

INTRODUCTION

We earlier reported that the proportion of hip injuries among all injuries to the knee/thigh/hip complex in frontal crashes has increased in modern vehicles (Wang, 2004; Sochor, 2003; Chong, 2007). This is of significant concern as hip injuries are clinically more severe and more difficult to treat than injuries to either the knee or the thigh. Pelvic fractures, particularly those involving disruption of the hip joint (acetabulum), often result in significant rehabilitation costs and long-term disability (NHTSA, 2005). Hip injuries frequently cause a lifelong impaired gait and account for the majority of life years lost due to motor vehicle crash knee-thigh-hip (MVC KTH) injuries (Pfeifer, 2011) .

Address correspondence to Sven Holcombe, International Center for Automotive Medicine, University of Michigan. Electronic mail: svenho@umich.edu

Posterior wall acetabular fractures in MVCs occur from posterior loading through the femoral head with the femur constrained during forward excursion of the pelvis. These mechanisms have been tested through cadaveric loading experiments, (Rupp, 2002; Salzar, 2006) and fracture risk curves have been developed (Rupp, 2010). One shortfall however is that such studies are limited to the cadaveric specimens available and suitable for testing – primarily elderly males – which may not be representative of the MVC population.

Field data analyses indicate that the distribution of injuries within the hip joint may depend on individual factors. For example, Wang et al. (2004) showed that males are more likely to receive posterior wall fractures than females, with analysis of CT scans from MVC occupants showing a bias towards increasing fractures with more laterally facing acetabular cups. Thus, a possible source for this gender dissimilarity in injury pattern is the presentation of the acetabular cup (acetabular anteversion), with males having more laterally facing acetabula than females.

Finite element analysis is a tool well suited to model the effects of the geometric variation seen in the population, provided accurate description of such variation is available. Current human finite element (FE) models can incorporate modifications in geometry and material properties in order to model the changes from anthropometric factors such as age or gender (e.g., Kimpara, 2005; Ito, 2009; El-Jawahri, 2010). Gross pelvic changes between genders are well documented and have been used to modify general pelvis size and shape using FE mesh morphing techniques (e.g., Li, 2007; Besnault, 1998). However, such general shape descriptions of the pelvis provide limited resolution around the acetabular wall. If indeed acetabular fracture likelihood is influenced by local shape changes, currently available geometry morphology data may not capture these local factors. Finite element modeling that incorporates finer resolution in the geometric shape changes of the relevant anatomical structures between the different MVC populations may elucidate important fracture risk indicators.

This study was undertaken to characterize the anatomic differences that affect hip injury tolerance and to do it on a smaller length scale with a larger sample population than has been attempted in the past. Its central hypotheses are that individual anatomic variations influence the degree of acetabular engagement of the femoral head, that these variations are at least partially related to gender, and that they have consequences for both the pattern of and tolerance to injury.

The specific aims of this study are to: (1) Demonstrate the significance of acetabular geometry on acetabular fracture; (2) Investigate the relationship between anthropometric measures such as gender, age, height, and weight with specific measures of acetabular geometry; (3) Develop a parametric predictive model for acetabular rim geometry based on gender, age, weight, and height through multivariate linear regression. As a consequence of aim (3), we hope to provide a data source from which to morph FE models of the acetabulum to specific population groups in order to investigate their responses to pelvic loading seen in MVCs.

METHODS

Standard medical pelvis computed tomography (CT) scans were used to take detailed measurements of human acetabular geometry from two populations. The first population was crash-injured patients studied at the University of Michigan's International Center for Automotive Medicine (ICAM) from 2000 to 2010. The second came from consecutively admitted University of Michigan trauma department patients between 2006 and 2010. All populations were limited to those 16 years or over who underwent a standard trauma protocol CT scan including the pelvis at the time of admission.

Of the population of crash-injured ICAM patients, any "driver" and "front seat passenger" occupants receiving pelvic fractures through any aspect of the left or right acetabulum were characterized as fractured. All planar (non roll-over) crash directions were included. Acetabular fractures to any non-MVC patients were accounted for (see geometry normalization, below); however these individuals were not included in the fractured group.

Base geometry extraction

For every scan, the location and size of each left and right femoral head was specified as a sphere having a centroid coordinate and nominal sphere radius. These were determined automatically using a best-fit sphere algorithm adapted from Cao, et al. (2006) using the standard Hough transform (SHT). Firstly, an SHT is calculated for each CT slice to identify the centers of planar circles in those images with radius between 10mm and 25mm. The two most prominent clusters of circle origins indicated approximate centers of the left and right femoral heads. From these central locations, a radial gradient filter was applied to the scan images to accentuate the outer cortical edges of the femoral heads (light areas, Figure 2b). A second SHT is then performed on these 2D filtered images to identify candidate planar circles of the femoral head. A best-fit sphere centroid coordinate and radius was then fitted to these planar circles as illustrated in Figure 2c.

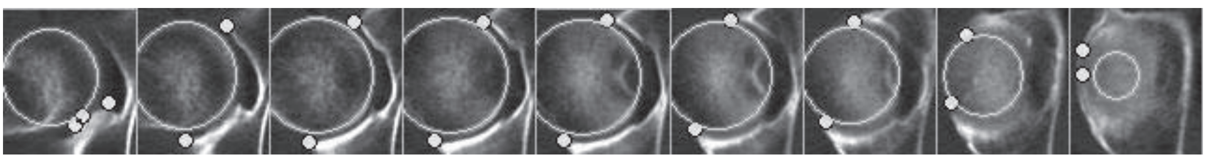

Figure 1: Axial slices through femoral head showing intersections with acetabular rim (dots). Slices move from inferior aspect (left) to superior aspect (right).

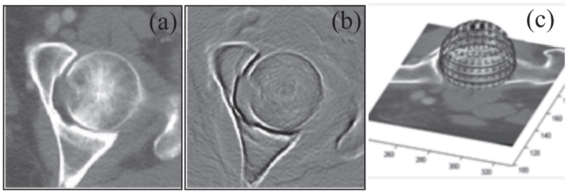

Figure 2: (a) Original CT axial slice (b) Radial-gradient filtered axial slice to accentuate outer cortical bone (c) Fitted sphere to planar circles

Next, a novel protocol was developed to extract acetabulum surface and rim pixels using a spherical coordinate system centered at one femoral head. Using this system, point samples of the scan pixels were taken at locations between 1.0 and 1.3 femoral head radii from the femoral head center using 3-dimensional tri-linear interpolation. This produced a spherically morphed volume with slices similar to that shown in Figure 3. Thresholding of the volume and its radial gradient (with 200 Hounsfield Unit and positive radial gradient thresholds), followed by edge and corner detection, identified any points lying on the acetabular rim as shown in Figure 3.

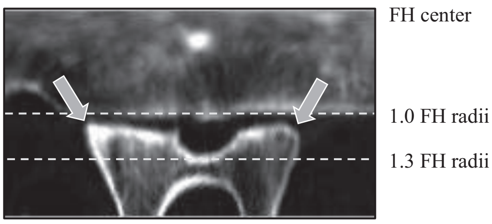

Figure 3: Radial slice from spherical volume. Top of image aligns with femoral head (FH) center. 1.0, and 1.3 FH radii are indicated by dotted lines. Arrows indicate intersection of image slice with the acetabular rim.

Extracted rim points of all scans were visually verified (Figure 1, Figure A1Figure A1:) on the left and right sides by operators blinded to patient data, with operators identifying cases where the automatic extraction process was unsuccessful. Examples of such cases include patients with excessive adduction whereby pieces of the femoral neck were recognized as acetabular rim, or patients with bone spurs recognized as acetabular rim (Figure A1d). In such cases, replacement of the acetabular rim was done using in-house MATLAB (The Math Works, Natick, MA) software whereby the operator would scroll through the axial images similar to Figure 1, placing rim points at the intersection of each slice and the acetabular rim.

Geometry normalization

Each acetabular rim point cloud was reduced to a closed loop of 100 interpolated rim coordinates sampled at 3.6 degree increments around an axis pointing from the femoral head center directly out of the acetabular cup. This axis was defined by rotating the lateral body axis 17.3 degrees around the superior axis, then -36 degrees around the anterior axis. These rotational constants were determined from the orientation of an average best-fit plane to points from all acetabular rim geometries. A transformation from scan-coordinates sc to acetabular-coordinates ac is represented by Equation (1), and from ac back to sc in Equation (2), using the definition for $\bar{\boldsymbol{R}}$ in Equation (3) as follows:

$$\begin{bmatrix} x_{ac} \\ y_{ac} \\ z_{ac} \\ 1 \end{bmatrix} = \bar{\boldsymbol{R}}^T \begin{bmatrix} x_{sc} \\ y_{sc} \\ z_{sc} \\ 1 \end{bmatrix} \quad \textbf{(1)}$$

$$\begin{bmatrix} x_{sc} \\ y_{sc} \\ z_{sc} \\ 1 \end{bmatrix} = \bar{\boldsymbol{R}} \begin{bmatrix} x_{ac} \\ y_{ac} \\ z_{ac} \\ 1 \end{bmatrix} \quad \textbf{(2)}$$

$$\bar{\boldsymbol{R}} = \begin{bmatrix} \cos -36 & 0 & -\sin -36 & 0 \\ 0 & 1 & 0 & 0 \\ \sin -36 & 0 & \cos -36 & 0 \\ 0 & 0 & 0 & 1 \end{bmatrix} * \begin{bmatrix} \cos 17.3 & \sin 17.3 & 0 & 0 \\ -\sin 17.3 & \cos 17.3 & 0 & 0 \\ 0 & 0 & 0 & 0 \\ 0 & 0 & 0 & 1 \end{bmatrix} \quad \textbf{(3)}$$

As illustrated in Figure 4, any given point can either be represented as a scan-based $[x_{sc}\ y_{sc}\ z_{sc}]$ (lateral/anterior/superior) coordinate from the femoral head center, an acetabular cup based $[x_{ac}\ y_{ac}\ z_{ac}]$ coordinates, or acetabular cup based spherical [θ φ ρ] coordinate. The azimuth (θ) gives the angle around the acetabular rim. The angle (φ) gives the elevation from the acetabular plane, and ρ gives the distance from the femoral head center.

In order to represent each individual with a single geometry, all right-sided geometries were mirrored, and each individual was given the average between his or her left-right geometry. Similarly, an individual's femoral head radius was given as the average of the left and right femoral heads. When a patient received unilateral acetabular or femoral head injuries, or if unilateral prosthesis hardware was present, only the uninjured side was used. When a patient's unilateral injury included dislocation of the femoral head from the acetabular socket, that femoral head location was replaced manually by a point at the center of the acetabular socket. This was done to retain realistic lateral axes directions for patients with hip dislocations. Patients with bilateral acetabular injuries or prostheses were excluded from the study.

Geometry shape factors

For each individual's geometry, a plane of best fit was calculated to represent the nominal acetabular plane. In order to avoid the out-of-plane influence from the non-articular acetabular notch, those points in the notch region as indicated in Figure 5 were excluded from the best-fit plane calculation. The notch region limits (18 to 120 degrees) were chosen to cover the peaks in φ and ρ seen at the notch region in Figure 5b. The angle between the normal of this fitted plane and the scan lateral axis gives the acetabular anteversion angle (AAA), as illustrated in Figure 6. Similarly, the angle between this plane and the inferior-to-superior axis gives the acetabular abduction angle (AAbA).

Statistical Analyses

Fracture Risk. Of the population of crash-injured patients studied at ICAM, 91 occupants with unilateral acetabular fractures were identified as having left-or right-sided fractures.

Initial univariate comparisons were made between the geometric shape factors (anteversion and abduction angles) of males and female, injured and uninjured, as well as injured/uninjured males and females separately. Subsequently, a multivariate logistic regression to the presence of fracture was performed using predictors of age, gender, height, weight, and acetabular anteversion angle (AAA).

Geometric Parametric Model. Generalized linear regression was used to predict 3-dimensional acetabular rim geometry from parameters of gender, age, height, and weight. To do this, a separate regression model was created for each of the 100 points around the acetabular rim. Spherical coordinates φ and ρ were used to isolate the shape changes in the acetabulum at each of the 100 given values of θ.

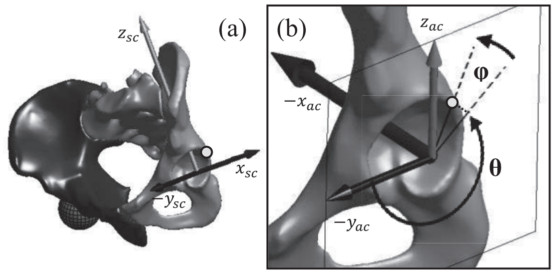

Figure 4: Acetabular rim points in (a) Scan coordinate system and (b) Acetabular plane coordinate system with spherical coordinates θ (rotation around x_{ac}) and φ (angular distance from $[x_{ac}\ y_{ac}]$ acetabular plane) for a given rim location (yellow dot). Note the arrow directions of y_{sc}, y_{ac}, and x_{ac}, which are each shown reversed for figure clarity

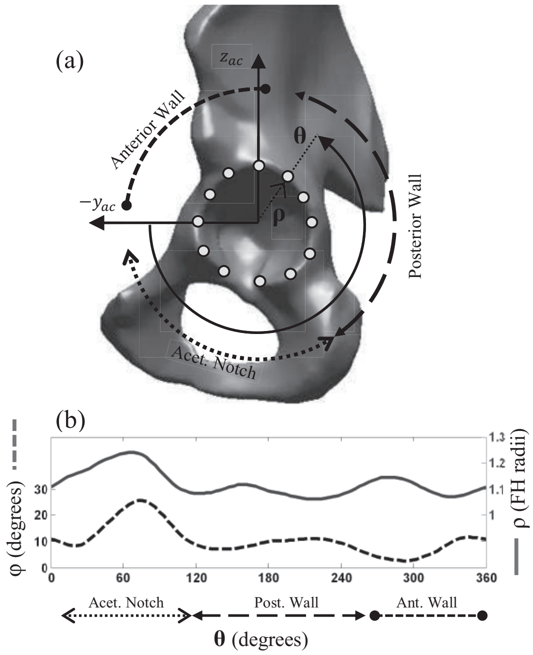

Figure 5: (a) Acetabular rim points at resampled locations around the acetabular axis (showing just 12 of 100 total θ and ρ locations for figure clarity) (b) Average φ and ρ across all individuals as a function of rim location θ. Dotted lines with arrows on (a) and (b) indicate approximate notch, anterior, and posterior rim regions

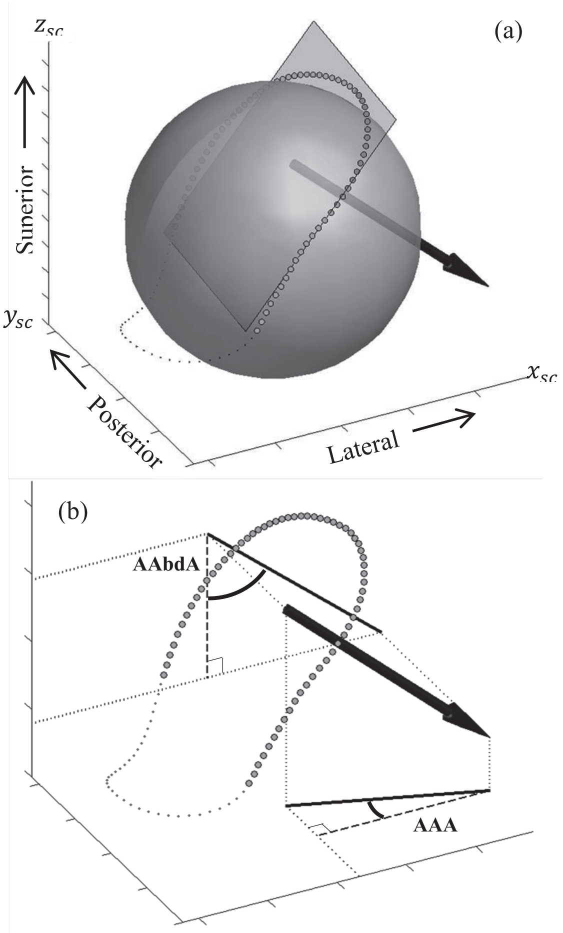

Figure 6: (a) Fitted plane to non-notch regions of the acetabular rim, with plane normal direction vector. (b) Acetabular anteversion angle (AAA) and abduction angle (AAbA), derived from plane normal vector angles between lateral and superior scan directions, respectively

RESULTS

1,150 individual geometries were measured (749 male, 401 female) from pelvis CT scans. Gender and age at the time of scan were known for all patients. Weight was known for 1,078 patients and height was known for 835. The distributions of known scan age, height, and weight are shown in Figure 7. Of the crash-injured occupants, 91 individuals (47 male, 44 female) received unilateral acetabular fractures. A comparison of the injured and uninjured populations is given in Table 1.

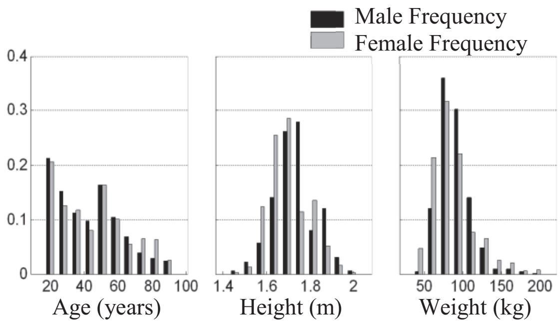

Figure 7: Male and female normalized frequency distributions of age, height, and weight

Table 1: Average age, height, weight comparison between injured and non-injured populations

Variable (units)	Male Fx.	Male No Fx.	Female Fx.	Female No Fx.
Age (years)	40	41	43	45
Height (m)	1.80	1.79	1.65	1.63
Weight (kg)	97	89	79	73

Acetabular anteversion angles and abduction angles were calculated for all patients, and are shown as frequency distributions in Figure 8. The average AAA for all males and females was 16.19±6.55 degrees and 18.84±7.68, respectively. Univariate t-tests of AAA between males and females, and fractured and non-fractured populations for each gender were performed, with box-plots of AAA from these populations given in Figure 9. All p-values showed significance at $p<0.001$, with fractured populations having lower anteversion angles than non-fractured populations. Equivalent tests using acetabular abduction showed no significance at the $p=0.05$ level.

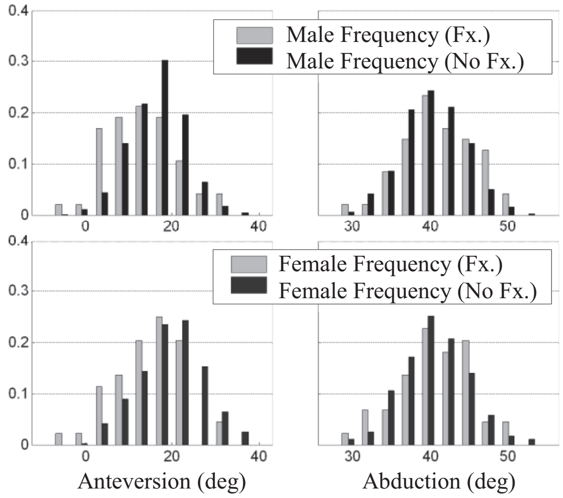

Figure 8: Male and female fractured vs. non-fractured frequency distributions of acetabular anteversion and abduction angles

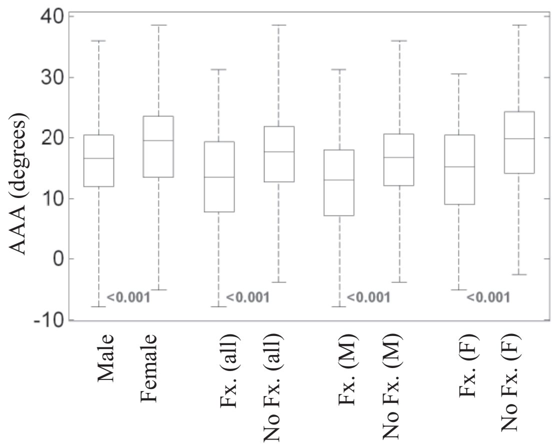

Figure 9: Box-plots of acetabular anteversion angle (AAA) for male, female, fractured and non-fractured populations. Boxes indicate median and 25th/75th percentiles, whiskers indicate data ranges. Univariate t-test *p*-values between adjacent populations are shown between boxes.

In order to assess the contribution of AAA to the likelihood of acetabular fracture, a multivariate logistic regression was performed to the presence of fracture [0 1], using the predictor variables of age, gender, height, weight, and AAA. Of these predictors, AAA had the lowest p-value ($p<0.001$), giving a fracture odds ratio increase of 8% for each one degree decrease in AAA. Regression results are summarized in Table 2.

Table 2: Logistic regression results of age, gender, height, weight and acetabular anteversion angle (AAA) to the presence of fracture

Factor (units)	Coeff.	Odd Ratio (%)	*p*-value
Age (yrs)	0.0015	1.0015	0.824
Sex (M=0)	0.9120	2.4893	0.008
Ht. (m)	0.5875	1.7988	0.727
Wt. (kg)	0.0104	1.0105	0.047
AAA (deg)	-0.0825	0.9208	<0.001

To assess the ability to predict acetabular angle by anthropometric parameters, a linear regression to AAA from parameters of gender, age, height, and weight was performed. This regression indicated predictive significance of age and weight ($p<0.001$), near-significance of gender ($p=0.09$) and no significance of height ($p=0.74$). Removing the height parameter from the regression allowed the inclusion of a greater number of observations (1,087), and increased the significance of all other parameters ($p<0.001$). This regression gives a multivariate model for anteversion angle (AAA, degrees) based on age (years), gender (SEX, M=0/F=1), and weight (WT, kg), as follows:

$$AAA = 16.06 + 0.107AGE + 1.43SEX - 0.047WT \quad \textbf{(4)}$$

The relationship between an individual's age, gender, and weight with the resulting acetabular rim shape was solved using a generalized linear model for φ and ρ at each rim geometry point. Full model coefficients are provided in Table A1 in the appendix, giving 100 values of φ and ρ as functions of age, gender, and weight. ρ has been normalized by femoral head radius. A graphical depiction of the model coefficients is provided in Figure 10 which shows, at any given acetabular rim location θ, the changes in φ and ρ that come about from each 10 year increase in age, 25kg increase in weight, or female-to-male difference. Triplets of [θ, φ, ρ] can be converted to scan-coordinates using (3) followed by a spherical-to-Cartesian transformation and then scaled by femoral head size.

Scaling by femoral head size can either be applied directly from a known value or obtained parametrically from anthropometric measures.

Despite gender being associated with femoral head radius in univariate tests, after accounting for height, weight, and age, neither gender nor its interaction with other variables remains significant. Therefore a multivariate model for femoral head radius (FHR, mm) was created based on height (HT, m, $p<0.001$), weight (WT, kg, $p=0.016$) and age (years, $p<0.001$), as follows:

$$FHR = -2.505 + 14.097HT + 0.005WT + 0.025AGE \quad \textbf{(5)}$$

The complete set of coefficients in Table A1 (Appendix) is available online for download through http://automotivemedicine.org/research/patterns.shtml. Furthermore, a custom-built MATLAB program is available from the link above, which provides both a command-line and graphical user interface to display and return Cartesian acetabular geometry parametrically from any given age, gender, height, and weight. Example parametric geometry created from two individuals (25yrs, 75kg male and 75yrs, 55kg female) is illustrated in Figure 11.

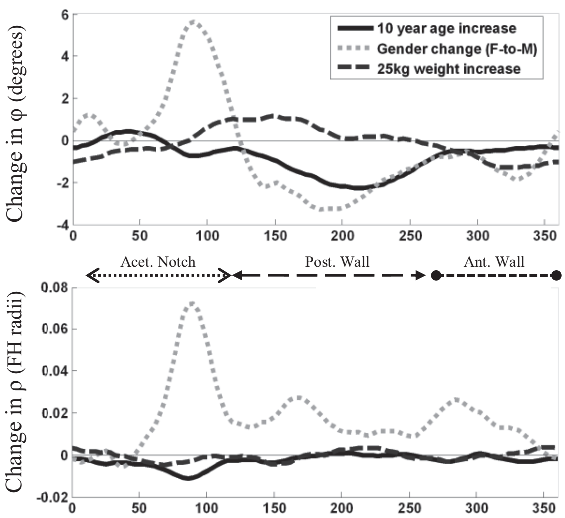

Figure 10: Magnitude of regression model changes in spherical out-of-plane rotation (Phi) and distance from femoral head center (Rho) with given adjustments to age, gender, and weight

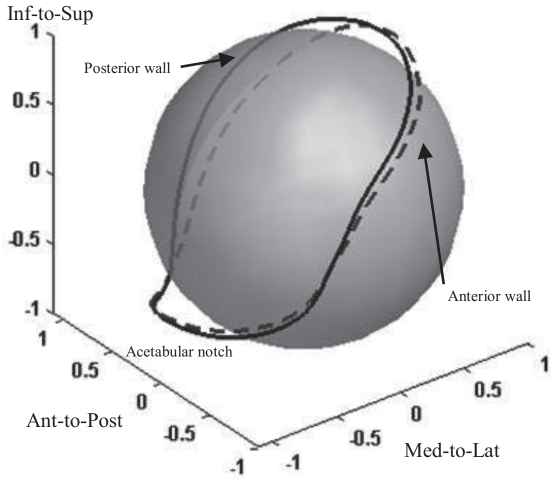

Figure 11: Comparison geometry of young male (25yrs, 75kg, solid line) to elderly female (75yrs, 55kg, dotted line) acetabular rim geometry

DISCUSSION

The use of CT scans is increasingly common in research and they have been used extensively in this study. The resolution of images used here range from 0.625mm to 2.5mm in slice thickness, and 0.3mm to 0.85mm in axial resolution. For the extraction of rim point locations, however, resampling of this voxel space was performed as described in the methods section above using tri-linear interpolation. Consequently, the geometric point locations of the acetabular rim are not constrained to the original CT volume pixel grid.

While a large and varied adult population of individuals has been included in this study, the parametric model produced is only valid for predicting geometry of individuals falling within the age, height and weight distributions given in Figure 7. This model is not aimed at predicting pediatric morphology.

Measurements of AAA presented in the current study are based on full 3-dimensional geometry of the acetabular rim. Clinical reports of anteversion angle are commonly based on a single axial slice near the center of the femoral head. In order to compare the current population to reported corridors, an equivalent measurement of planar AAA was taken using only two of 100 acetabular rim points nearest the axial level of the femoral head center. This scheme is equivalent to basing AAA measures on only the central panel of Figure 1. Comparison of this planar AAA measure against reported values from

100 individuals in Stem, et al. (2006) is provided in Figure 12. Current results have been separated into equivalent age and gender groups and match reported corridors well. It is thought that this study's marginally lower results for planar AAA are due to a lower mean age of this study's individuals within each comparison group. The 3-dimensional AAA and planar AAA values are highly correlated, with a Pearson's linear correlation coefficient of 0.94. The choice to use AAA based on full 3-dimensional geometry rather than two planar points for this study's statistical analyses was made because the intent of the study is to provide data useful to drive 3-dimensional model geometry.

When determining the importance of AAA on fracture risk, logistic regression was performed using AAA and anthropometric factors. The potential co-linearity between AAA and age, for example, is a valid concern, with a Pearson's linear correlation coefficient between the predictors of 0.303. To investigate this, comparative logistic regressions were performed with the inclusion/exclusion of AAA. Including AAA in the model gives a likelihood ratio test statistic of 22.8, which follows Chi-square with 1 degree of freedom, indicating a better fitting model as presented in the results, Table 2 ($p<0.01$). Since AAA is only a summary characteristic of acetabular shape, future efforts at functional statistical models of shape incorporating the presence of fracture may help highlight other factors of acetabular shape that influence fracture likelihood.

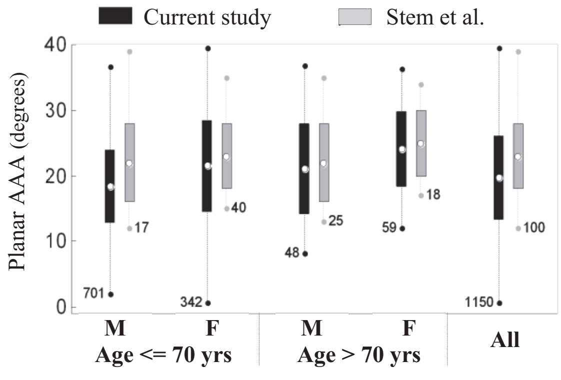

Figure 12: Comparison of mid-femoral head planar acetabular anteversion angle between Stem (2006) and the current study. Dotted lines indicate data ranges, boxes indicate data mean ± 1 SD. Data counts are indicated next to each lower range

While AAA has been associated with both gender and fracture occurrence, results here indicate that the geometric variation seen is not adequately modeled by a simple rotation of the acetabular cup to match anteversion angle. Instead, Figure 10 shows that as anthropometric factors change (particularly age and gender), the posterior wall portion of the acetabular rim experiences a larger magnitude in shape change than other rim areas. An example of this localized difference is shown in Figure 11 which compares the acetabular rim geometry of a young male and elderly female.

Morphologic differences in spherical coordinate ρ (the rim distance from the femoral head center, normalized by femoral head size) are also illustrated in Figure 10. These show changes primarily driven by gender, with males having over 2% greater distance to most parts of the rim, independent of their larger femoral head size.

The methods presented here account for pelvis lateral rotation by first adjusting the lateral scan axis to align with a left-to-right femoral head axis. When dislocation of one femoral head occurred, that femoral centroid point was replaced with a manually placed acetabular centroid location to define the left-to-right axis. Despite this step, it is possible that a substantially distorted pelvis with large shift of the whole injured side may alter the lateral vector of the uninjured side. Consideration was given to excluding pelves with severe distortion however there was difficulty in quantitatively defining "severe". The authors' subjective selection of the ten most distorted pelves did not produce statistically significant differences in AAA to the remaining fractured group.

In fracture categorization, non-MVC patients with acetabulum fractures from other forms of trauma were excluded from the fractured pelves group. This was chosen to highlight injuries directly relevant to MVCs. It is possible that acetabular geometry also plays a role in other forms of acetabular injury however that role is not the focus of this study.

The current study does not distinguish between specific crash directions. The effect of acetabular geometry on injury mechanism is likely to differ between frontal and side loading conditions. The statistical analyses performed in this study aim only to identify if local geometry is an important factor in acetabular injury, rather than quantify this importance between specific crash orientations. Future examination of fracture patterns from different crash directions may help illuminate this phenomenon.

Pelvic lordosis is not explicitly controlled for beyond patients being scanned in a supine position. Indeed lordotic variation is known to exist in the population, and aligning each pelvis anterior axis – for example via a pubis-to-sacral-foramen axis – may influence patient-to-patient geometry normalization (Kakaty, 2010; Tannast, 2007). We chose not to adjust geometry this way since the model is aimed for use in motor vehicle occupant modeling, in which we reasoned that any inter-patient variation in pelvic lordosis that is present in a supine position is likely also present in a seated occupant position. Studies of acetabular abduction angle have shown a Spearman's correlation of 0.378 between supine and seated orientations (Lazennec, 2010).

In the parametric model of rim shape, local sharp geometric details such as acetabular notch shape become smoothed by the contributions from the large sample size. This model is intended to be used as a basis for the morphing of a standard pelvic geometry to match a wide range of individuals, rather than the source geometry of those individuals itself. Similar methods are presented for other areas such as the rib cage (Gayzik, 2008) with general mesh morphing methods examined by Sigal et al. 2008.

Furthermore when used in the context of fracture prediction, model geometry is just one of a number of relevant factors. The current study is limited in scope to the morphology of the acetabular rim and how it differs throughout the population. In order to supply modelers with more complete data to study acetabular injury, future efforts should also be aimed at quantification of material properties such as strength and thickness of the acetabular bony geometry and how these properties vary with anthropometric factors.

CONCLUSION

Using 3-dimensional geometry extracted from CT scan volumes of 1,150 individuals, we have developed a representation of acetabular rim shape based on a femoral head-centered coordinate system.

Logistic regression to the presence of fracture using predictors that include summary shape factors show that acetabular fracture likelihood is significantly influenced by acetabular anteversion angle, with each 1 degree reduction in angle corresponding to an 8% increase in fracture likelihood.

We have presented a statistically significant model of acetabular rim size and shape as predicted by age, gender, height and weight. Full model coefficients and geometric transformations are provided, along with a software program to produce acetabular geometry parametrically from given anthropometric inputs. The parametric model is based on a broad population of live human subjects and is intended as numeric data for morphing of pelvis finite element models to produce appropriate local acetabular geometry known to affect fracture likelihood.

ACKNOWLEDGMENTS

The authors wish to acknowledge the contributions and assistance of Shije Cai, Lucy Hully, Mike Yee and Zuoping Li.

REFERENCES

Besnault, B., Lavaste, F., Guillemot, H., Robin, S., Le Coz, J. (1998) A Parametric Finite Element Model of the Human Pelvis. 42nd Stapp Car Crash Conference Proceedings: 337

Cao, Y., Ye, H., Doessel, O., Liu, C. (2006) Spherical parameter detection based on hierarchical Hough transform. Pattern Recognition Letters, 980-986

Chong, M, M Sochor, K Ipaktchi, C Brede, C Poster, S Wang. (2007). The interaction of 'occupant factors' on the lower extremity fractures in frontal collision of motor vehicle crashes based on a level I trauma center. J Trauma 62(3): 720-729.

El-Jawahri, R., Laituri, T., Ruan, J., Rouhana, S., Barbat, S. (2010) Development and Validation of Age-Dependent FE Human Models of a Mid-Sized Male Thorax. Stapp Car Crash Journal 54:407-30.

Gayzik, F.S., Yu, M.M., Danelson, K.A., Slice, D.E., Stitzel, J.D. (2008). Quantification of age-related shape change of the human rib cage through geometric morphometrics. J. Biomech. 41 (7), 1545–1554.

Ito O., Dokko Y., and Ohashi K. (2009) Development of Adult and Elderly FE Thorax Skeletal Models. Society of Automotive Engineers Paper 09B-0107, Warrendale PA, pp. 1-18.

Kakaty DK, Fischer AF, Hosalkar HS, Siebenrock KA, Tannast M. (2010) The ischial spine sign: does pelvic tilt and rotation matter? Clin Orthop Relat Res; 468(3):769-74

Kimpara H, Iwamoto M, Watanabe I, Miki K, Lee J, Yang K, King A. (2005) Effects of bodyweight, height, and ribcage area moment of inertial on blunt chest impact response. Proc. Int. Res. Council on the Biomech Impact (IRCOBI), pp 175-185.

Lazennec J, Boyer P, Gorin M, Catonne Y, Rousseau MA. (2010) Acetabular Anteversion with CT in Supine, Simulated Standing, and Sitting Positions in a THA Patient Population. Clinical Orthopaedics and Related Research; 469:4, 1103-1109

Li Z, Kim, JE, Davidson JS, Etheridge BS, Alonso JE, Eberhardt A.W. (2007) Biomechanical response of the pubic symphysis in lateral pelvic impacts: a finite element study. J. Biomech. 2007;40(12),2758-2766.

NHTSA, P Dischinger, KM Read, JA Kufera, TJ Kerns, SM Ho, CA Burch, N Jawed, AR Burgess. (2005). Consequences and Costs of Lower-Extremity Injuries. Baltimore, MD, CIREN Center, National Study Center for Trauma and EMS: 1-36.

Pfeifer, R, BA Zelle, P Kobbe, M Knobe, RL Garrison, S Ohm, NA Sittaro, C Probst, HC Pape. (2011). "Impact of Isolated Acetabular and Lower Extremity Fractures on Long-Term Outcome."J Trauma.Epub ahead of print: 23 May 2011.

Rupp, J.D., Reed, M.P., Van Ee, C.A., Kuppa, S., Wang, S.C., Goulet, J.A., Schneider, L.W. (2002). The tolerance of the human hip to dynamic knee loading. Stapp Car Crash Journal 46, 2122

Rupp, J.D., Flannagan, C., Kuppa, S. (2010). An injury risk curve for the hip for use in frontal impact crash testing, Journal of Biomechanics, Volume 43, Issue 3, Pages 527-531

Salzar RS, Bass CR, Kent R, Millington S, Davis M, Lucas S, Rudd R, Folk B, Donnellan L, Murakami D, Kobayashi S (2006) 'Development of Injury Criteria for Pelvic Fracture in Frontal Crashes', Traffic Injury Prevention, 7: 3, 299 — 305

Sigal, I., Yang, H., Roberts, M.D., Crawford Downs, J. (2010) Morphing methods to parameterize specimen-specific finite element model geometries, Journal of Biomechanics, Volume 43, Issue 2, Pages 254-262

Sochor, MR, DP Faust, SC Wang, LW Schneider. (2003). Knee, thigh and hip injury patterns for drivers and right front passengers in frontal impacts.SAE 2003 World Congress.Detroit, Michigan, SAE International.

Stem, E., O'Connor, M., Kransdorf, M., Crook, J. (2006). Computed tomography analysis of acetabular anteversion and abduction. Skeletal Radiology, 35: 6, 385-389

Tannast M, Siebenrock KA, Anderson SE. (2007). Femoroacetabular impingement: radiographic diagnosis - what the radiologist should know. AJR Am J Roentgenol;188(6):1540-52

Wang, SC, C Brede, D Lange, C Poster, ALange, C Kohoyda-Inglis, M Sochor, K Ipaktchi, S Rowe, S Patel, H Garton. (2004). Gender Differences in Hip Anatomy: Possible Implications for Injury Tolerance in Frontal Collisions. Annual Proceedings for the Association for the Advancement of Automotive Medicine, AAAM.

APPENDIX

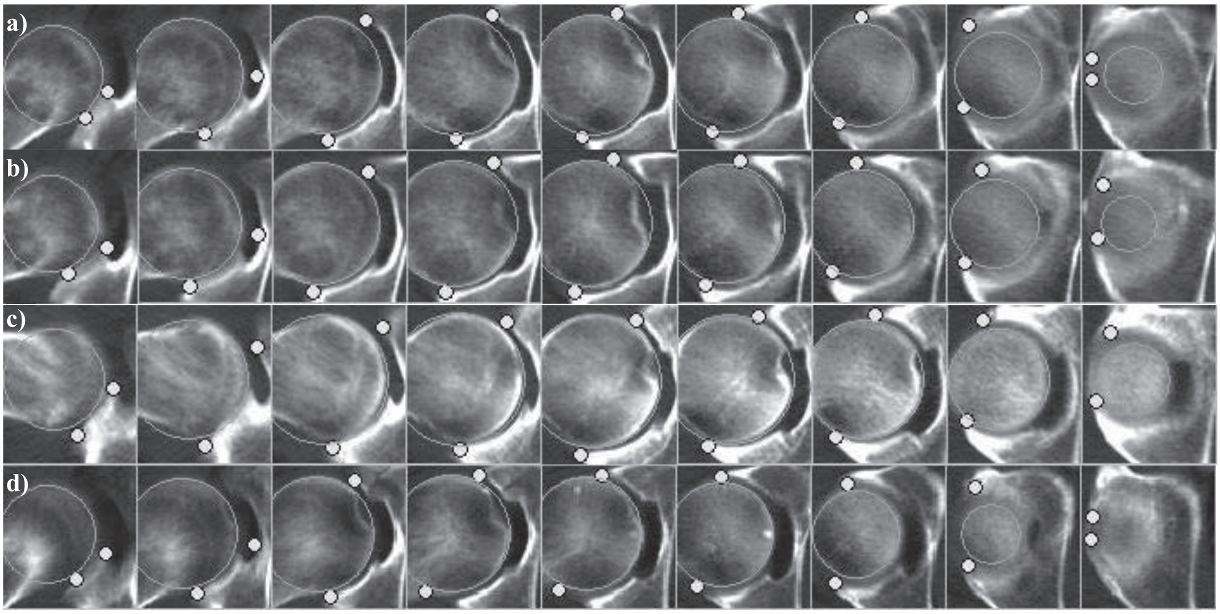

Figure A1: Rows of acetabular rim and femoral head images from 4 representative cases. Slices move from inferior aspect (left) to superior aspect (right). Circle indicates femoral head nominal sphere. Dots indicate intersection between slice plane and acetabular rim. (a) and (b): uninjured patient left and right (mirrored) sides. (c) Uninjured right side (mirrored) from patient with left acetabular fracture. (d) Patient with high hip adduction requiring manual correction of acetabular rim points. Note the placement of the automatic acetabular rim points falling on the femoral neck in panels 4, 5, and 6.

Table A1: Acetabular rim spherical coordinates model, left side

	Phi (ϕ, degrees)				Rho (ρ, FH radii)			
Theta	Const. *1*	Age *1 x 10⁻⁵*	Sex *1 x 10⁻²*	Weight *1 x 10⁻⁵*	Const. *1*	Age *1 x 10⁻⁵*	Sex *1 x 10⁻²*	Weight *1 x 10⁻⁵*
0	0.273046376	-5.830631194	0.71942516	-7.126388237	1.104982609	-1.885267076	-0.170441988	1.382893159
3.6	0.262766661	-5.694225957	1.262452781	-6.909559225	1.115342355	-1.944221104	-0.239775451	1.194035094
7.2	0.245332701	-4.890407395	1.841187804	-6.675907024	1.128470555	-1.859828933	-0.361190537	0.830407855
10.8	0.224295511	-3.714679726	2.099198219	-6.407739885	1.142062228	-2.15486574	-0.290549789	0.677958097
14.4	0.203713663	-2.046298976	2.043749975	-6.056019941	1.153882577	-2.665106258	-0.194152243	0.666833306
18	0.187933177	-0.061108654	1.792615072	-5.813251604	1.165346899	-3.403077719	-0.025805144	0.565153186
21.6	0.17714069	2.024178752	1.295679995	-5.306952534	1.17455565	-4.120578912	0.114406403	0.495099069
25.2	0.173756055	3.916386243	0.689636397	-4.59133311	1.179005492	-4.339662075	0.214765807	0.611406531
28.8	0.18079038	5.086990341	0.117039697	-3.965768342	1.184566058	-3.936469379	0.050444238	0.524653478
32.4	0.193338235	6.273025806	-0.243463738	-3.474688223	1.196689639	-3.544984129	-0.352108277	0.008858665
36	0.213897578	7.006597645	-0.343071406	-3.347820154	1.207991804	-3.56815986	-0.570562254	-0.144400994
39.6	0.238138254	7.350382934	-0.341772815	-3.294065564	1.218895471	-3.687886923	-0.523563348	-0.256776295
43.2	0.263223592	7.193885096	-0.080784257	-3.066613231	1.230476029	-3.872134115	-0.327946453	-0.575627033
46.8	0.289746874	6.931592822	0.213659768	-2.901737181	1.240139969	-4.228860089	0.027305162	-0.76733974
50.4	0.319830294	6.130527841	0.582543143	-2.897072882	1.2476043	-4.404681422	0.373850723	-0.955728225
54	0.348996143	5.269988473	0.88943893	-2.850126371	1.254909833	-4.612956186	0.72552502	-1.18787084
57.6	0.378394215	4.097470454	1.252559171	-2.859174214	1.262663592	-4.907333979	0.99447937	-1.483412618
61.2	0.407510326	2.618332212	1.732319332	-2.955012401	1.26766121	-5.290396009	1.350615586	-1.560021936
64.8	0.434494343	0.872268108	2.349356567	-3.026000822	1.273155575	-5.960530531	1.841711706	-1.732870642
68.4	0.453999324	-1.480039506	3.295765457	-2.577230694	1.276380827	-6.815174118	2.511204091	-1.878873787
72	0.466620172	-4.216149983	4.593526499	-2.040365718	1.274749379	-7.838118073	3.439980719	-1.839480171
75.6	0.468453593	-6.688784183	6.173120754	-1.451242258	1.267357144	-8.991090916	4.574597975	-1.598190424
79.2	0.464305954	-9.101171671	7.693323456	-1.172237902	1.256797106	-10.13535284	5.691891188	-1.433047772
82.8	0.449585908	-11.20346331	8.972581348	-0.704821075	1.242401701	-10.9559967	6.666255035	-1.35468547
86.4	0.422653896	-12.47732244	9.657209458	0.062019202	1.223600514	-11.028551	7.15011134	-1.23349961
90	0.384940582	-12.79787875	9.859749334	1.244621663	1.203510792	-10.89959281	7.203227785	-1.073415741
93.6	0.344913494	-12.74171659	9.561259722	2.300635064	1.179288806	-9.953757316	6.871813444	-0.731137988
97.2	0.300545953	-12.02619302	9.056908605	3.44365107	1.156927898	-8.740321463	6.155567788	-0.457241718
100.8	0.25747937	-11.02971862	8.387224417	4.449880616	1.138388575	-7.404093217	5.211072771	-0.425741834

104.4	0.218846614	-10.13195479	7.466715884	5.211086981	1.121956434	-6.016286953	4.132533837	-0.25298592
108	0.183868096	-9.113749608	6.290029055	5.890801569	1.109579907	-4.766368449	3.225878103	-0.209613648
111.6	0.156558364	-8.292687583	5.104074757	6.363247039	1.101270041	-3.52424787	2.425838694	-0.342864871
115.2	0.134592555	-7.446781188	3.62127756	6.781401151	1.095668133	-2.747088588	1.865252241	-0.381417498
118.8	0.120260819	-6.934513351	2.063559452	7.050477386	1.093201501	-2.503523968	1.569350004	-0.461690508
122.4	0.114477312	-6.887684464	0.5681936	6.955422342	1.091646235	-2.556693321	1.511978219	-0.326570604
126	0.116177529	-7.917264448	-0.754500499	6.719515468	1.091383717	-2.452082824	1.451637834	-0.242816658
129.6	0.117442078	-9.154545083	-1.776545278	6.893782512	1.095059839	-2.391323446	1.33962033	-0.439857649
133.2	0.124096714	-10.59086804	-2.581026895	6.744090813	1.097135431	-2.255737293	1.290720022	-0.4098279
136.8	0.129459511	-11.98949533	-3.289089452	6.860654496	1.103083237	-2.447307589	1.413739558	-0.615275241
140.4	0.133268708	-13.03239601	-3.795106039	7.009278302	1.112366437	-3.154851729	1.570810454	-0.840925839
144	0.132475551	-14.06870282	-3.778762536	7.652363293	1.124869147	-3.669619398	1.568111886	-1.409296083
147.6	0.138145507	-15.66989581	-3.666492445	7.887990448	1.13294773	-3.732929021	1.685897238	-1.708396164
151.2	0.148299068	-17.60014937	-3.519267387	7.893458082	1.136250188	-3.550584885	1.84658066	-1.732662557
154.8	0.163725844	-19.40881968	-3.732284468	7.421810177	1.135710171	-3.252489575	2.139279328	-1.527952367
158.4	0.181080303	-21.91259499	-4.042017026	7.26207878	1.134682692	-2.507364547	2.399875848	-1.672641475
162	0.197181173	-23.93564752	-4.256341803	7.249539953	1.12890941	-2.023166661	2.624556844	-1.399301151
165.6	0.21388825	-25.67205749	-4.435934719	7.03828749	1.119365406	-1.518498423	2.701726672	-0.86293856
169.2	0.228810183	-27.16635734	-4.692887192	6.918267974	1.109370665	-1.080236772	2.734829687	-0.444648977
172.8	0.246619483	-28.11168845	-5.05436918	6.299913262	1.099793763	-0.778082273	2.619702465	-0.101227644
176.4	0.267638892	-29.03521621	-5.440779772	5.335082909	1.092210484	-0.639133128	2.416472261	0.103159456
180	0.28916083	-30.56612557	-5.614289343	4.306548084	1.086221677	-0.504317578	2.19771781	0.194877554
183.6	0.305790508	-32.66604968	-5.719613517	3.627861778	1.08144456	-0.074108939	1.976199302	0.099177591
187.2	0.319575617	-35.03161268	-5.706912821	3.111790126	1.078873471	0.351225585	1.738586226	-0.064351072
190.8	0.333282214	-36.68794201	-5.695255711	2.305155331	1.074719859	0.661808282	1.502586977	0.105339289
194.4	0.346834504	-37.59808534	-5.654962947	1.371012987	1.067081409	0.921056779	1.336629876	0.599665963
198	0.357354947	-38.11896089	-5.641680909	0.800325766	1.061109401	0.876212117	1.176265432	0.909013172
201.6	0.362955442	-38.3937886	-5.545525771	0.652840749	1.056903331	0.871843354	1.113255821	0.963432239
205.2	0.368222339	-38.741131	-5.350851609	0.546658255	1.051747624	0.967501149	1.095425652	1.084519353
208.8	0.372837828	-39.2459765	-5.163885547	0.49365351	1.049175888	0.697540923	1.070311334	1.154112468
212.4	0.372819742	-39.6223999	-4.867775532	0.825326632	1.047042355	0.241579587	1.084128596	1.401147385
216	0.369251247	-39.45569697	-4.624222278	1.090438482	1.047692574	0.001748736	0.968005741	1.388204645
219.6	0.365615229	-39.05666468	-4.262605357	1.085991254	1.04893942	-0.137473945	0.935668174	1.319422097
223.2	0.36046674	-38.47806341	-3.967957448	1.025942875	1.050156256	-0.220970396	1.008695348	1.264588981
226.8	0.349597477	-37.4705911	-3.538003069	1.28320225	1.051923499	-0.391743541	1.134283328	1.272372837
230.4	0.338111466	-36.30327	-3.31644191	1.424077559	1.055359272	-0.304352496	1.146620259	1.121629929
234	0.326631897	-34.65166187	-3.124679662	1.11307089	1.060847215	-0.278895005	1.138224552	0.826725292
237.6	0.314626145	-32.80463755	-2.989956024	0.568573717	1.065269631	0.013706185	1.157966975	0.629697122
241.2	0.298005548	-30.89459162	-2.808408698	0.383751848	1.071988762	0.126167774	1.138987341	0.411558499
244.8	0.275996947	-28.82162497	-2.529734581	0.581023165	1.082041338	0.1153262	1.025940815	0.00352599
248.4	0.257302507	-26.67048145	-2.405565964	0.332375993	1.092324336	0.208468288	0.913989188	-0.35924501
252	0.237868377	-24.44745898	-2.308846787	0.031709106	1.103341166	-0.095261984	0.878666942	-0.556873284
255.6	0.218107256	-22.07710986	-2.119257678	-0.355144041	1.114331385	-0.486122021	0.917462014	-0.671580218
259.2	0.199849431	-19.55235529	-1.918181579	-0.97673894	1.123804553	-0.992331917	1.127820853	-0.63217498
262.8	0.179818122	-17.0445058	-1.669791977	-1.316556614	1.132586053	-1.3220932	1.366735818	-0.622616449
266.4	0.161451123	-14.67888834	-1.535853887	-1.521945871	1.140543595	-1.826263438	1.595866707	-0.534266669
270	0.146917491	-12.60624212	-1.447069987	-1.846298421	1.149099665	-2.365490045	1.873726239	-0.689520217
273.6	0.137959549	-11.12940822	-1.37487233	-2.343172997	1.155556189	-2.754464535	2.138192978	-0.859036055
277.2	0.132595805	-9.897059776	-1.436597787	-2.961571337	1.161800668	-3.214815491	2.344404763	-1.204415379
280.8	0.128441004	-9.205065374	-1.363167389	-3.374440767	1.16040483	-3.127820719	2.512177515	-1.182985604
284.4	0.126679125	-8.862804289	-1.224349586	-3.855120933	1.154574355	-2.662302279	2.629252815	-1.02437672
288	0.125101257	-8.879711784	-1.094190819	-4.066037012	1.147239175	-2.002232616	2.590045233	-0.842511593
291.6	0.124439772	-9.097912474	-0.936944845	-4.167780546	1.140328913	-1.311835017	2.44137302	-0.728691182
295.2	0.129272249	-9.365008047	-1.02425968	-4.592736848	1.132822894	-0.490551479	2.231299624	-0.775928595
298.8	0.14014763	-9.549582948	-1.238244234	-5.39246382	1.120556442	0.282448378	2.096023326	-0.470109632
302.4	0.154687328	-9.549047705	-1.401638304	-6.288884273	1.108535798	0.553204598	2.040903143	-0.133683096
306	0.172249122	-9.379206635	-1.686524078	-7.340321452	1.101098694	0.274570319	1.886638235	-0.08038507
309.6	0.187880377	-8.853453422	-2.008773405	-8.108979547	1.097287943	-0.338396858	1.654724543	-0.169608932
313.2	0.205182026	-8.533937843	-2.384244439	-8.688057915	1.093786752	-1.030132278	1.449007577	-0.204558836
316.8	0.220667868	-8.365117199	-2.619412349	-8.876661507	1.089636548	-1.392764897	1.328778066	-0.324077729
320.4	0.236339857	-8.043623254	-2.749920288	-8.958058095	1.08324602	-1.722139256	1.331024392	-0.150784892
324	0.252698633	-7.382672385	-3.019292857	-9.06113717	1.077233088	-2.142879816	1.297594712	0.256401014
327.6	0.271210863	-7.128236476	-3.268765322	-9.126685992	1.075665501	-2.675447776	1.213870114	0.34413835
331.2	0.28567603	-6.738282454	-3.228843253	-9.044004005	1.076319796	-3.13850071	1.179057542	0.41250534
334.8	0.295477841	-6.501285658	-2.973981328	-8.683928071	1.078140527	-3.327516764	1.033734896	0.481496561
338.4	0.303814924	-6.052553118	-2.765662009	-8.65315529	1.080700011	-3.313428792	0.785610087	0.585439525
342	0.306405229	-5.790840417	-2.257738693	-8.505365078	1.080351655	-3.039863922	0.624455695	1.038440847
345.6	0.304090886	-5.42730508	-1.695256121	-8.37965547	1.082339173	-2.585982596	0.36876859	1.301502078
349.2	0.296370548	-5.416404618	-1.106350421	-7.896199509	1.08611366	-2.229572964	0.142464665	1.440324525
352.8	0.287226812	-5.643603281	-0.490926877	-7.410383053	1.091485318	-2.050296293	0.006273289	1.498309763
356.4	0.279047982	-5.760264812	0.170704335	-7.190587215	1.097735128	-1.938280086	-0.114309211	1.464238571
360	0.273046376	-5.830631194	0.71942516	-7.126388237	1.104982609	-1.885267076	-0.170441988	1.382893159